Christopher P. Fredlake[1]
Daniel G. Hert[1]
Thomas P. Niedringhaus[2]
Jennifer S. Lin[3]
Annelise E. Barron[3]

[1]Department of Chemical and Biological Engineering, Northwestern University, Evanston, IL, USA
[2]Department of Chemical Engineering, Stanford University, Stanford, CA, USA
[3]Department of Bioengineering, Stanford University, Stanford, CA, USA

Received December 13, 2011
Revised January 26, 2012
Accepted February 2, 2012

Research Article

Divergent dispersion behavior of ssDNA fragments during microchip electrophoresis in pDMA and LPA entangled polymer networks

Resolution of DNA fragments separated by electrophoresis in polymer solutions ("matrices") is determined by both the spacing between peaks and the width of the peaks. Prior research on the development of high-performance separation matrices has been focused primarily on optimizing DNA mobility and matrix selectivity, and gave less attention to peak broadening. Quantitative data are rare for peak broadening in systems in which high electric field strengths are used (>150 V/cm), which is surprising since capillary and microchip-based systems commonly run at these field strengths. Here, we report results for a study of band broadening behavior for ssDNA fragments on a glass microfluidic chip, for electric field strengths up to 320 V/cm. We compare dispersion coefficients obtained in a poly(*N,N*-dimethylacrylamide) (pDMA) separation matrix that was developed for chip-based DNA sequencing with a commercially available linear polyacrylamide (LPA) matrix commonly used in capillaries. Much larger DNA dispersion coefficients were measured in the LPA matrix as compared to the pDMA matrix, and the dependence of dispersion coefficient on DNA size and electric field strength were found to differ quite starkly in the two matrices. These observations lead us to propose that DNA migration mechanisms differ substantially in our custom pDMA matrix compared to the commercially available LPA matrix. We discuss the implications of these results in terms of developing optimal matrices for specific separation (microchip or capillary) platforms.

Keywords:
Band broadening / Dispersion / DNA sequencing / Microchip electrophoresis / Polymer matrix
DOI 10.1002/elps.201100686

1 Introduction

The electrophoretic separation of DNA in polymer networks continues to be of substantial significance as the basis for an important and still ubiquitously used analytical tool in the biological sciences. The determination of the sequence of the human genome[1, 2] gave scientists an invaluable resource for guiding future medical and biotechnology research, and the continued advancement of DNA sequencing technologies toward lower cost promises benefits to public health. While lower throughput DNA sequencing and genotyping assays are still typically carried out by capillary array electrophoresis (CAE), microfluidic chip-based electrophoresis systems are being developed and are expected to speed analysis and reduce overall cost per lane.

A tremendous advantage of microchip DNA separations lies in its use of a cross-channel injection geometry [3] to decrease the initial peak width and ultimately reduce the necessary separation distance to achieve highly accurate and long sequencing read lengths. Several research groups are pursuing the development of integrated devices for genetic analyses that combine both the preparation and the analysis of biological samples [4–10]. These integrated bioanalysis systems will bring down sample processing costs, by allowing a reduction in total assay time (both in sample preparation and sample analysis), and these instruments will reduce capital cost by replacing two separate instruments with a single,

Correspondence: Professor Annelise E. Barron, Department of Bioengineering, Stanford University, 318 Campus Drive, James H. Clark Center, Room W300B, Stanford, CA 94305-5444, USA
Email: aebarron@stanford.edu
Fax: +650-723-9801

Abbreviations: **BRM**, biased reptation model; **DMA**, *N,N*-dimethylacrylamide; **GPC**, gel permeation chromatography; **HEA**, *N*-hydroxyethylacrylamide; **LPA**, linear polyacrylamide; **MALLS**, multi-angle laser light scattering

multifunctional unit. So far, there has not been much work done toward developing tailored DNA sieving matrices and microchannel wall coatings specifically for use on microchips; much more work has been done on the development of the instrumentation and hardware. It seems to have been assumed by many that commercially available separation networks for DNA sequencing and genotyping in fused silica capillaries can be used in glass or plastic microchips. However, we have recently shown that this is not the case for DNA sequencing [11].

To analyze the separation of DNA fragments, we can consider the resolution of the separated peaks, which is the ratio of the peak spacing to the average of the peak widths. The peak spacing can be recalculated as the selectivity of the matrix, which describes the mobility of each fragment in the matrix and can be predicted as a function of fragment size, matrix characteristics, and local electric field strength by physical mechanistic models, such as Ogston sieving [12–14] and biased reptation models (BRM) [15–17]. The temporal peak widths (FWHM in units of time), W_t, of DNA fragments are also dependent on the fragment mobility, μ, and local electric field strength, E, but are also related to the total variance, σ_{tot}^2, in the system [18]:

$$W_t = 2[2\ln 2]^{\frac{1}{2}} \frac{\sigma_{tot}}{\mu E} \quad (1)$$

Therefore, minimizing the total variance in the system would also minimize the temporal peak widths of each fragment of DNA, maximizing the resolution of the separation. The total variance is the sum of the individual contributions to the variance that originate from the injection of the sample, the finite detection volume in the microchip or capillary, the thermal gradients across the microchannel, and diffusion of the DNA in the separation matrix. Considering that the microchip used in this study has a smaller internal diameter than the capillary used in the study by Luckey et al., and thus a larger surface area to volume ratio, it is reasonable to neglect the contributions to the peak widths from thermal gradients and finite detection volumes that were determined to be negligible in comparison to the contributions from the injection plug width and zone dispersion [18]. Thus, the total variance for capillary systems can be expressed as:

$$\sigma_{tot}^2 = \frac{w_{inj}^2}{12} + 2D_E t_r \quad (2)$$

where w_{inj} is the injection plug width, t_r is the migration time for a fragment from injection to detection, and D_E is the apparent dispersion coefficient, which encompasses both Brownian diffusion from random thermal motion and electric field-induced fragment dispersion. Chip-based separation devices were designed specifically to minimize injection widths to 100 μm or less, so that dispersion is the main contributor to peak broadening during chip electrophoresis [19].

Of peak spacing and peak broadening, peak spacing has generally been more thoroughly studied experimentally and theoretically (through separation mechanism modeling). However, while both experiments show and biased reptation theory predicts that DNA mobility will become size independent at some critical fragment length, in practice, peak widths limit the resolution on most DNA separations, even if the mobility is still changing with fragment size [20]. Since peak broadening is such a crucial parameter for increased band resolution, it is surprising that only a limited number of studies have addressed DNA band broadening specifically. BRM does actually predict a change in the dispersion coefficient's dependence on DNA size and electric field strength for different "regimes" of the model [21], and Tinland et al. experimentally verified the predictions of Slater's model for the dispersion coefficient at low electric field strengths (<20 V/cm) [22–26]. Similarly, other reports have also attempted to study band broadening and the dispersion coefficient at low electric field strengths [27–32], but the applicability of these results to capillary or chip-based separation systems that generally employ higher field strengths (150–300 V/cm) is likely low. Studies of band width at these larger field strengths are even rarer, with only a few papers discussing band widths at all when optimizing DNA fragment resolution during electrophoresis in either gels [18, 33–35] or linear polymer solutions [19, 36].

In this paper, we report on DNA band broadening behavior for ssDNA fragments under sequencing (denaturing) conditions in a microfluidic chip with electric field strengths up to 320 V/cm. Specifically, we compared DNA dispersion coefficients in a poly(*N,N*-dimethylacrylamide) (pDMA) matrix developed in our lab specifically for chip-based DNA sequencing with those obtained in a commercially available linear polyacrylamide (LPA) developed for high-quality DNA sequencing separations on a CAE instrument. We measured much larger dispersion coefficients for the DNA fragments in the LPA matrix relative to the pDMA matrix. Additionally, the change in dispersion coefficient with both DNA size and electric field strength were quite different in the two matrices, leading to the conclusion that the DNA migration mechanisms are likely different within the two polymer networks. We then discuss the implications of these results in terms of developing matrices for specific separation platforms.

2 Materials and methods

2.1 Polymerization

pDMA and poly(*N*-hydroxyethylacrylamide) (pHEA) were synthesized by aqueous-phase free-radical polymerization as described previously [37]. The DMA monomer (Monomer-Polymer, Dajac Labs, Feasterville, PA, USA) and HEA monomer (Lonza, Walkersville, MD, USA) were dissolved to 5% (w/w) and 0.5% (w/w) concentrations, respectively, in deionized water. The solutions were deoxygenated with bubbling nitrogen for 45 min at 47°C. The reactions were initiated by adding 0.003 g of V-50 (2,2'-azobis(2-amidinopropane) dihydrochloride, Wako Chemicals (Richmond, VA, USA) per

100 mL of monomer solution. The reactions were allowed to proceed for 6 h after which the polymer solutions were dialyzed against distilled, deionized water for 2 weeks with frequent water changes. The purified polymer was then recovered by lyophilization.

2.2 Polymer characterization

Polymer average molar masses and molar mass distributions were determined by tandem gel permeation chromatography (GPC) (Waters, Milford, MA, USA)-multi-angle laser light scattering (MALLS) (Wyatt Technology, Santa Barbara, CA, USA) as described elsewhere[38]. Polymer solutions were prepared at a concentration of 1.0 mg/mL in the GPC aqueous mobile phase (0.1 M NaCl, 50 mM NaH_2PO_4, and 200 μM NaN_3). The samples were fractionated on the Waters Separations Module 2690 GPC using Shodex (New York, NY, USA) OHpak columns SB-806 HQ, SB-804 HQ, and SB-802.5 HQ connected in series. The GPC columns were used to fractionate a dilute, polydisperse polymer sample (the columns can fractionate polymers between 30 kDa and 8 MDa in molar mass). As the monodisperse fractions eluted from the column (with larger molar masses eluting first), the MALLS system used a refractive index detector to determine fraction concentration and a light scattering detector to quantify molar mass. The molar mass distributions were determined by using the Astra software from Wyatt Technology, using an assumption of 100% sample recovery from the columns.

2.3 Dynamic coating of chip microchannels

The creation of an adsorbed polymer film coating onto the internal borosilicate glass surfaces of microchips was described previously [39]. Prior to adsorption of polymer chains onto the channel surface from aqueous solution, the walls were treated with 1 M aqueous HCl by filling the channel and letting the solution remain in contact with the surface for 15 min. Following acid treatment, the channels were flushed with water. A 0.1% (w/v) solution of the coating polymer, pHEA (M_w = 2.1 MDa) was then introduced into and held in the channels for 15 min. The polymer solution is then removed by vacuum followed by a water wash through the channels.

2.4 Microchip-based DNA separations

Separations of ssDNA ET-900 ladder (Amersham Biosciences, Piscataway, NJ, USA) were carried out on a custom-built four-color sequencing system using isotropically etched single-channel borosilicate glass microchips with a channel depth of 20 μm, a 7.5-cm effective separation distance, and a 100-μm offset T injection scheme. These chips were purchased from Micronit Microfluidics BV (Enschede, The Netherlands). The separation and detection system have been previously described in detail by Chiesl et al. 39]. Briefly, the system consists of an electrical subsystem and an optical subsystem along with a temperature control setup for the microfluidic chips. The spectrum of the filtered light is measured by directing it through a transmission grating and focusing it onto a high quantum efficiency, 532 × 64-pixel charge-coupled device (CCD) cooled to −15°C (Hamamatsu, Bridgewater, NJ, USA).

Separations of a ssDNA ladder was carried out in pDMA that was dissolved in 1 × TTE (49 mM Tris, 49 mM TAPS, and 2 mM EDTA) plus 7 M urea; separations were also carried out in the commercially available LongRead™ LPA matrix that was developed for DNA sequencing in the MegaBACE system (purchased from GE Healthcare/Amersham, Piscataway, NJ, USA). The DNA sample consisted of ET dye-labeled fragments ranging in size from 60 to 900 bases with fragments differing in size by 25 bases beginning with the 75-base fragment (i.e. fragment sizes 75 bases, 100 bases, 125 base, etc.). DNA of 60, 310, and 610 bases were also included in the ladder for a total of 37 peaks to be detected. For each run, an electric field at the same strength as the separation was applied for 60 s prior to sample injection ("prerun electrophoresis"), for the purpose of moving any charged small-molecule contaminants out of the matrix. An offset T injector with 100 μm offset was used and the sample was injected for 40 s at 500 V/cm. Separations were carried out at electric fields ranging from 150 V/cm to 320 V/cm, with 150 V/cm back-biasing applied to the sample and sample waste wells to eliminate sample leakage during the separation. The chip was maintained at 50°C for the duration of the run using a temperature controller connected to a copper heating plate. The peak centers and peak widths were determined using Peak Fit v4.06 (SPSS, Chicago, IL, USA).

3 Results and discussion

3.1 Microchip electrophoresis of ssDNA fragments

An ssDNA ladder consisting of 37 fragments ranging in size from 60 to 900 bases was separated in a microchip electrophoresis system in both a 4% (w/v) pDMA (M_w = 5.9 MDa) dissolved in 1 × TTE plus 7 M urea and the commercially available LongRead™ sequencing matrix, a highly entangled and high-molar mass LPA solution. Figure 1 shows a typical separation of the ssDNA ladder in both of these matrices using a 7.5-cm separation distance and an applied electric field strength of 235 V/cm. All of the fragments in the ladder are well resolved in both matrices, although the largest 3–4 fragments in the LongRead™ matrix are not resolved to baseline.

The separations shown in Fig. 1 can be evaluated quantitatively by calculating both the selectivity per base and the average FWHM of the peaks. Figure 2 plots both the selectivity and average FWHM versus DNA size; each data point is plotted at the larger of the two fragments used to calculate the selectivity and the average FWHM. These quantities were calculated from the average of three separate

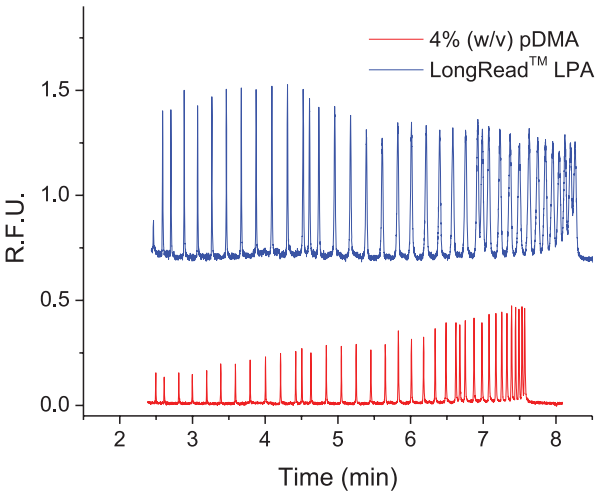

Figure 1. This figure shows typical electropherograms of the ssDNA ladder separated in both the 4% pDMA matrix and the LongRead™ LPA matrix. For calculations and analysis of the separations, three replicate runs for each matrix were completed. The separation conditions for each matrix include a temperature of 50°C, an electric field strength of 235 V/cm, an effective separation distance of 7.5 cm in a borofloat glass chip, and a surface coating of dynamically adsorbed pHEA. The sample consisted of 37 ssDNA fragments of different lengths, labeled with a covalently attached ET dye (Amersham/GE Healthcare). The DNA size range is from 60 to 900 bases. The peak spacing starting from the second peak (75 bases in size) is 25 bases. Additional peaks are found at 310 bases and 610 bases.

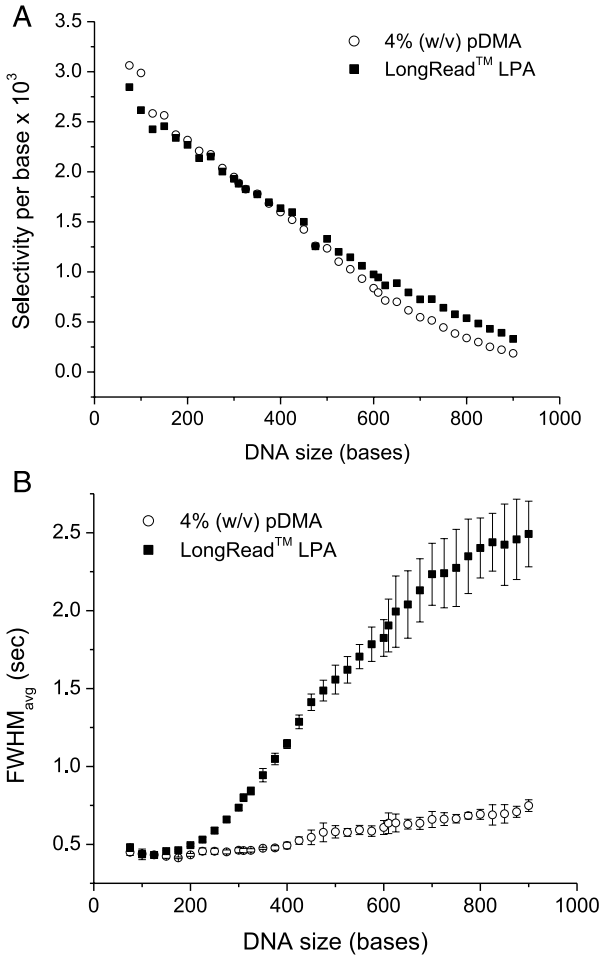

Figure 2. Both the (A) selectivity and the (B) average peak FWHM of the ssDNA ladder separations are plotted versus DNA size. The data points are plotted at the larger DNA size of the two peaks for which selectivity and average FWHM are calculated. These values are calculated for average values of the mobility and peak widths for three separate electrophoresis separations with conditions the same as in Fig. 1. Error bars for the selectivity were smaller than the size of the data points and were omitted.

runs, and the relative standard deviation of the migration times was approximately 1% or lower. For DNA sizes smaller than 150 bases in Fig. 2A, the selectivities are higher in the pDMA matrix than in LongRead™, while the selectivities are nearly equal in the two matrices for DNA ranging in size from 150 to 400 bases. For fragments larger than 400 bases, the LongRead™ matrix is more selective than the pDMA matrix.

In Fig. 2B, the average FWHM is approximately equivalent in both matrices for DNA sizes up to 200 bases. However, for DNA fragments larger than 200 bases, the average FWHM increases significantly with fragment size in LongRead™ matrix relative to the pDMA matrix. In previous microchip studies, our group has shown that under the same separation conditions as in Fig. 1, a 4% (w/v) pDMA matrix with a molar mass of 3–5 MDa can deliver DNA sequencing read lengths of 550 bases on a chip [37], while the LongRead™ matrix can only sequence DNA up to 300 bases or less [11]. From the data in Fig. 2, one can conclude that although the selectivity of the LongRead™ matrix may be equivalent to or better than the pDMA matrix for DNA sizes up to 550 bases, the resolution and sequencing read lengths are lower in LongRead™ because of much wider DNA peak widths than those observed in the pDMA matrix.

3.2 DNA dispersion coefficients during electrophoretic separations

The peak widths plotted in Fig. 2B are the averages of the measured peak widths from three separate runs in each matrix. As can be seen in Fig. 1, the mobilities of the DNA fragments in the two matrices are not the same, with the DNA molecules taking a longer time to move through the LongRead™ matrix than through the pDMA matrix. Although measured widths of the bands passing the detector are a function of migration time (Eqs. (1) and (2)), we can use the measured peak widths to calculate the apparent dispersion coefficients of DNA bands in the two matrices. Rearranging Eq. 2 and substituting into Eq. 1 gives:

$$D_E = \frac{1}{2t_r}\left[\frac{(W_t \mu E)^2}{8 \ln 2} - \frac{w_{inj}^2}{12}\right] \quad (3)$$

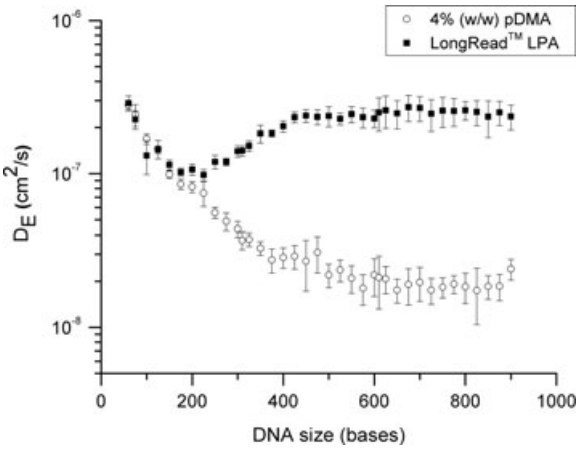

Figure 3. The DNA dispersion coefficients, D_E, are shown for ssDNA fragments electromigrating through the polymer matrices under conditions described in Fig. 1. The dispersion coefficients were calculated using Eq. (3). Error bars were calculated from standard error propagation formulas using the standard deviations for both the measured migration time and final peak width of each fragment.

By calculating D_E, we can quantify the extent of peak broadening in the two matrices even though migration times of the DNA fragments are different. Note that we are calculating the apparent dispersion coefficient, which combines the effects of Brownian diffusion with the effects of dispersion due to the electrophoresis of DNA through the polymer matrix. While some studies have attempted to measure these two effects separately [18, 28], we believe the apparent dispersion coefficient is a more practical quantity to use because these effects are not separable for experimentalists developing and optimizing electrophoresis systems.

We calculated the apparent dispersion coefficients for the DNA fragments moving through both matrices, which are shown in Fig. 3 (for brevity in the remainder of the paper, we will drop the term "apparent" before dispersion coefficient, although D_E will continue to represent the combined effects of Brownian motion and electrophoretic dispersion). Despite the fact that peak widths are seen to increase with increasing DNA fragment size in Fig. 2B, the dispersion coefficients are actually decreasing relative to increasing DNA size for the pDMA matrix. This is due to the fact that the peak widths are measured in units of time and the peaks that correspond to larger DNA fragments move more slowly than peaks corresponding to smaller DNA fragments. Ultimately, these larger DNA fragments remain in the detection zone longer and thus have wider temporal peaks. However, the mobility and migration time of each peak are taken into account when calculating the dispersion coefficient (Eq. (3)) so that the true dispersion during the electrophoretic separation (due to Brownian motion and electrophoresis effects) is illustrated.

Knowing this, a decrease in the DNA dispersion coefficient with increasing DNA size may then be an expected result in the LongRead™ matrix. In contrast, the calculated DNA dispersion coefficients actually increase with increasing DNA size in the range from 250 to 500 bases. At DNA sizes larger than 500 bases, the dispersion coefficients change very little in LongRead™. The DNA dispersion coefficients are not only greater in the LongRead™ matrix than in the pDMA solution, but for fragments larger than approximately 200 bases, the change in D_E with DNA size follows a substantially different trend in the two networks, indicating that the migration dynamics ("mechanism") of the DNA fragments in the two matrices differ significantly.

3.3 DNA separation mechanism considerations

In the framework of the BRM, Slater calculated the dependence of DNA size on the diffusion coefficient, or the dispersion coefficient in this study, for different "regimes" of biased reptation [21, 40]. In the limit of very small electric field strengths, the dispersion coefficient scales with DNA size (N) as N^{-2} for very small DNA fragments. For slightly larger fragments in the reptation regime, the dispersion coefficient scales as N^{-1} in the "reptation–equilibrium" regime and then scales as $N^{-0.5}$ in the "accelerated–reptation" regime. As the size of DNA fragments continue to increase, the DNA ultimately aligns with the electric field in the "oriented reptation" or "reptation-plateau" regime and the dispersion coefficient scales as N^0. For oriented reptation of DNA, the mobility also scales as N^0 so that separation of fragments is no longer possible. These predictions have been confirmed experimentally for very low fields in cross-linked gels [22–24], but at higher field strengths, such as those used in capillary or microchip electrophoresis, quantitative confirmation is lacking since these field strengths lie outside of the assumptions of the BRM theory.

The DNA dispersion coefficients in the LongRead™ matrix shown in Fig. 3 are surprising because nowhere in the BRM theory is the dispersion coefficient predicted to increase with DNA size, even though there have been experimental reports showing that static interactions with the separation matrix can cause an increase in peak widths for analytes during electrophoresis [41, 42]. In fact, a mechanism for DNA migration in gels has been described in the literature, which would lead to static analyte–matrix interactions. Deutsch and Madden termed this mechanism "geometration", which they described for large dsDNA molecules moving through cross-linked gels [43, 44]. In this mechanism, the center of the DNA molecule "hooks" onto a fiber in the gel, and both ends of the DNA are stretched by the electric field so that the molecule forms a "U-shaped" conformation with the DNA-gel contact point at the apex of the "U". Eventually, one of the two extended arms "wins" the tug-of-war, and pulls the other arm back around the DNA-gel contact point and the

molecule disengages from the matrix (Supporting Information Fig. S1). Geometration has been observed experimentally by videomicroscopy in cross-linked gels [45], physically cross-linked polymer solutions [46], and microfabricated post-based obstacle courses [47]. Popelka et al. calculated the expected dispersion coefficient of DNA undergoing geometration and have shown that this mechanism does lead to an increase in dispersion coefficient with an increase in DNA size [48]. For PFGE separations, the geometration mechanism was identified as a possible explanation for the observed increase in diffusion coefficient with increasing DNA size [49].

Although the geometration mechanism has been attributed only to large dsDNA (>2 kbp), this mechanism may also be adopted for smaller sized ssDNA. The Kuhn length of dsDNA is approximately 300 bp [50], so molecules smaller than approximately 1 kbp are probably not flexible enough to form the U-shaped conformation when interacting with the matrix. However, ssDNA has a much shorter Kuhn length of approximately 30 bases [51] making these molecules very flexible at sizes common to sequencing fragments (up to 1000 bases). Thus, the formation of these U-shaped conformations necessary for geometration should be possible, based on the flexibility of the DNA chains, for many of the ssDNA fragment sizes used in this study.

Previously, we have hypothesized a mechanism for ssDNA migration through a pDMA matrix, which is a hybrid mechanism of transient entanglement coupling (TEC) [52,53] and reptation[37]. In this mechanism, DNA initially hooks onto entanglements in the matrix in a manner similar to the first steps of the geometration mechanism, but instead of getting caught and remaining in place, the DNA pulls polymer chains out of the entangled matrix and through the solution while remaining in the U-shaped conformation. In an effort to compare the dispersion data plotted in Fig. 3 with our previously hypothesized mechanism, the mobility of DNA fragments in the pDMA matrix and LongRead™ matrix were plotted against DNA size (Supporting Information Fig. S2). The trends in the mobility data suggest three migration regimes are present in both polymer matrices: the Ogston-like sieving regime, the unoriented biased reptation regime, and the oriented biased reptation regime. These are the traditional physical mechanistic models that have been previously reported when considering mobility data alone [20, 37, 40]. However, as previously discussed, the trends in the dispersion coefficient data do not suggest the presence of these migration mechanisms in the LongRead™ matrix. An explanation for this observation is that the LongRead™ matrix is a much more viscous and highly entangled matrix compared to the pDMA matrices developed in our group [11]. In the more "robust" (more strongly entangled) LPA network, it is possible that the DNA migration mechanism is altered and the DNA molecules cannot pull the polymer chains out of the established network. As a result, DNA fragments are held static in the U-shaped conformation and continue to move forward only after disengaging from the matrix. In the end, these results imply that the difference in separation resolution may result from the effects that the migration mechanism has on band broadening through DNA chain length-dependent variation in the dispersion coefficient (Fig. 3) rather than the effects that the DNA migration mechanism has on DNA fragment mobility or selectivity (Supporting Information Fig. S2).

3.4 Electric field influence on DNA dispersion coefficients

The electric field strength can affect peak widths in a variety of ways. Increasing the field strength can reduce the time needed for separation and, therefore, give the DNA fragments less time for dispersion. However, Luckey and Smith have shown that higher field strengths (above 200 V/cm) can lead to additional peak broadening because Joule heating can create a radial temperature profile leading to increased variance in the DNA fragment mobilities [33]. To make the matter more complicated, Slater has shown that, from the BRM theory, the dispersion coefficient of DNA actually increases at higher electric field strengths for all but the smallest fragments [21]. In fact, Slater argues that Luckey and Smith have actually overestimated the peak broadening effect of Joule heating at higher field strengths, and that any increase in the peak widths with an increase in electric field strength results from the dependence of the dispersion coefficient on the field strength, which in turn results from differences in DNA migration mechanism [54].

For our initial separations, an electric field strength of 235 V/cm was chosen, since this was found empirically to be the optimal electric field strength for chip-based DNA sequencing separations in our pDMA matrices. To examine the effect of the field strength on DNA dispersion coefficients in both the 4% pDMA matrix and the LongRead™ LPA matrix, ssDNA separations were carried out at electric field strengths ranging from 150 V/cm to 320 V/cm, which are commonly used field strengths for capillary- and microchip-based DNA separations. The DNA dispersion coefficients in the pDMA matrix at different field strengths, as shown in Fig. 4A, do not change much for DNA sizes lower than 300 bases, but an increase in the dispersion coefficient is seen for the larger fragments as the field strength is increased.

The dispersion coefficients of the DNA fragments in the LongRead™ matrix are shown in Fig. 4B. The DNA size at which the dispersion coefficients begin to increase shifts to smaller sizes as the field strength is increased. Even at 150 V/cm, which is below the 200 V/cm threshold where Luckey and Smith postulated that heating effects caused increased peak broadening [33], there is an increase in the dispersion coefficient with DNA size for fragments larger than ~300 bases. Due to this, we conclude that abnormal heating effects are not responsible for the large increase in dispersion coefficients with DNA size

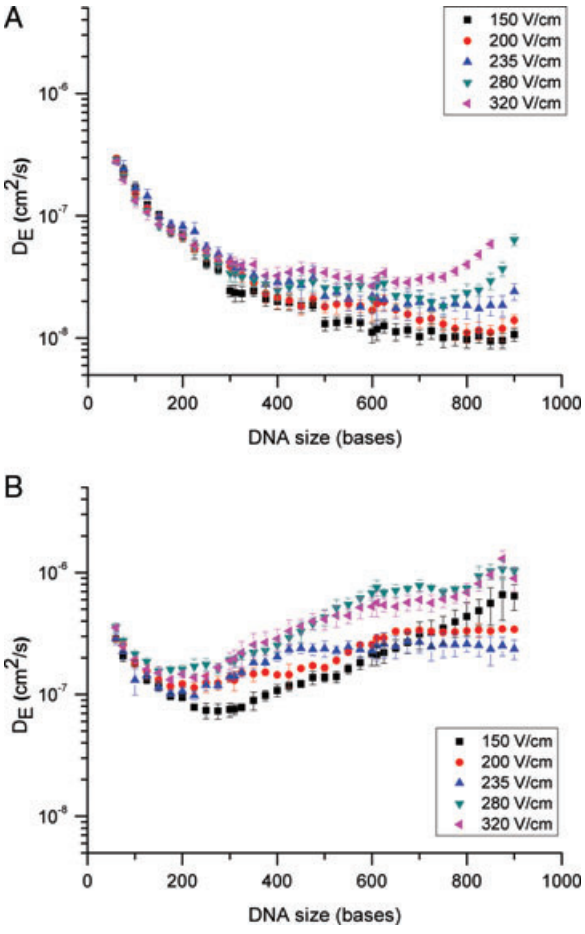

Figure 4. The DNA dispersion coefficients, D_E, are shown for different electric field strengths for DNA electromigrating through (A) 4% (w/v) pDMA matrix and (B) LongRead™ LPA matrix. Other separation conditions are identical to those described in Fig. 1. Error bars were calculated using standard error propagation formulations using the standard deviations for both the migration time and the final peak width of each fragment.

in this matrix. Ultimately, we assert that the difference in the observed trends in the DNA dispersion coefficients between the two matrices is the result of the difference in DNA migration mechanisms in the two polymer networks.

3.5 Comparing DNA separations in microchips and capillaries

We have shown that the DNA dispersion coefficients for DNA greater than 250 bases in size are much larger during electrophoresis through LongRead™ LPA than through a 4% pDMA matrix. This leads to much better sequencing performance with the pDMA matrix than with the LongRead™ matrix in a microchip using conditions identical to those used in this study [11, 37]. However, the LongRead™ matrix can deliver read lengths of 800 bases or greater on the MegaBACE 1000, a commercial CAE sequencing instrument, while use of the 4% pDMA matrix results in read lengths of approximately 650 bases (data not shown). The disparate results in the microchips and the CAE instrument imply that there are differences between separations in capillaries and those in microchips. However, the local environment for the DNA molecules as they move through a matrix should be identical whether the separation is occurring in a capillary or a microfabricated channel in a glass chip, so that the mobilities and dispersion coefficients should be the same regardless of the separation platform.

The main difference between chip and capillary separation platforms is the sample injection method. For capillaries, direct electrokinetic injection is used, and the initial plug width depends on the DNA mobility, electric field strength, and the injection time [18]:

$$w_{inj,cap} = \mu \times E_{inj} \times t_{inj} \quad (4)$$

For accurate sample detection, a sufficiently high concentration of DNA must be initially injected into the capillary. In order to increase the injected DNA concentration from a sample, either the electric field or the injection time can be increased. However, an increase in either of these parameters leads to an increase in initial plug width, which leads to a decrease in separation efficiency (and increased separation lengths needed to maintain the same resolution or read length) [19]. In microchips, the cross injector (or offset T injector), was designed such that smaller initial sample plug widths could be injected into the separation channel, which increases the separation efficiency so that shorter separation distances can be used to good effect.

For very small injection plug widths, the dispersion of DNA zones is the only contributor to peak broadening during separations. Therefore, a matrix such as the LongRead™ will require much longer separation distances than the 4% pDMA in a microchip because of the much larger dispersion coefficients of DNA fragments in the LongRead™ matrix. However, in capillaries, if the initial injection plug is rather large, DNA dispersion may be less influential overall on the final peak width of the bands, and, therefore, separation performance depends less on DNA dispersion coefficients in the matrix and more on matrix selectivity.

To illustrate this argument, we can calculate the approximate distance that a DNA fragment band can be expected to broaden during an electrophoresis experiment [18]:

$$d_{disp} = \sqrt{D_E t_r} \quad (5)$$

The retention time, t_r, depends on the mobility of the DNA fragment and the separation distance, for which we will use either 7.5 cm for a microchip or 50 cm for a capillary separation in this example. We will assume an injection width

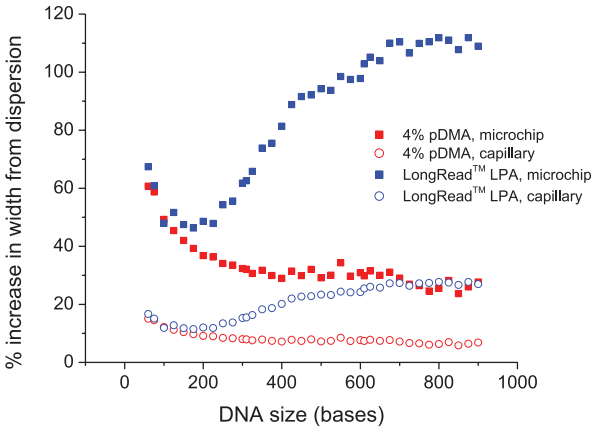

Figure 5. Using the same mobilities and dispersion coefficients measured in the two matrices used in this study, the percentage increase of the final peak widths over the initial peak widths are calculated for DNA moving either through a 7.5-cm microchip or a 50-cm capillary. In the calculations used to generate this plot, the initial sample plug widths are assumed to be 100 μm in the microchip and 1 mm in the capillary. The percentage increase is calculated as the distance a DNA fragment will disperse during electromigration (Eq. (5)) divided by the initial plug width.

on a chip of 100 μm, and an injection plug width of 1 mm in the capillary. All other conditions (e.g. temperature, surface coating, electric field strength, etc.) are assumed to be identical, such that the DNA mobility and dispersion coefficients calculated in this study can be used to determine the increase in the final peak widths resulting from DNA dispersion over the initial peak width. Figure 5 shows the results of this calculation for separations in both a capillary and a microchip in the two matrices used in this study. In capillaries, the pDMA matrix still contributes less to the overall peak widths than the LongRead™ because of the lower dispersion coefficients, but even the largest fragments in the ladder moving through the LongRead™ matrix would only increase in final peak width by approximately 30% over the initial injection plug width. For separations in microchips, however, the dispersion of DNA in the LongRead™ matrix increases the final peak widths to over 100% of the initial plug width for the larger DNA fragments, while the pDMA matrix only increases the final peak width of these fragments to 30–40% over the initial width.

This analysis demonstrates the relative importance of knowing the DNA dispersion coefficients in a polymer solution when designing a separation matrix for a microchip device. Conversely, when a system has larger sample injection widths, such as in a capillary, the system can be optimized with little knowledge of the dispersion coefficients. Thus, a high-performance matrix developed for capillary-based instruments may not be capable of the same high-quality DNA separations (for DNA longer than 200 bases) in microchips, and the implication is that materials for microchip-based DNA separations must be specifically designed and tested for these new miniaturized platforms.

4 Concluding remarks

Band broadening of DNA zones during electrophoretic separations at conditions typical of capillary or microchip-based instruments has been given sparse attention in the literature, even though most DNA separations are limited in practice by the widening of the detected bands. While DNA mobility in a matrix is a relatively easy parameter to measure, the extent of band broadening of DNA fragments during electrophoresis is just as important to understand when developing new separation matrices, especially for microchip-based separation platforms.

The LongRead™ matrix is a highly entangled and high-molar mass LPA solution that performs well on capillary-based instruments such as the MegaBACE 1000. This type of matrix has often been considered the archetype of a high-performance sequencing matrix, and a similar type of matrix has delivered the longest DNA sequencing read (1300 bases) ever published [55]. However, as sequencing and genotyping technology becomes miniaturized so that complete analytical systems can be included on a single borosilicate chip [6, 7, 10], the need for materials designed specifically for these platforms will grow. We have shown that the dispersion coefficients of DNA electromigrating through polymer matrices can differ depending on the matrix, and we hypothesize that the migration mechanism for DNA through these entangled networks is the cause. Ultimately, understanding the DNA migration mechanism and how it relates to the properties of a separation matrix is the key when developing materials for chip-based electrophoretic DNA separations.

Resolution and read lengths can be increased, in most cases, by lengthening the channel, and some research groups have used this approach when developing microfabricated systems in lieu of further optimization of separation matrices [56]. However, the choice of a good sequencing matrix such as the pDMA solution employed in this study can reduce the required separation distances and times relative to a matrix such as LongRead™. Therefore, the availability of newly designed materials for DNA separations on microchips should provide better, and truly optimal performance of these systems and help usher in the next generation of long-read electrophoretic DNA sequencers and genotyping instruments, which while being lower in throughput than next-generation DNA sequencing technologies, will surely find uses for which they are ideal.

This work was supported by grant No. 2 R01 HG001970-07 and No. 1 RC2 HG005596 from the National Human Genome Research Institute of the National Institutes of Health. The views expressed in this manuscript are solely the responsibility of the

authors and do not represent the official view of the National Human Genome Research Institute or the National Institutes of Health. Finally, the authors thank Professor Gary W. Slater for helpful discussions.

The authors have declared no conflict of interest.

5 References

[1] Lander, E. S., Linton, L. M., Birren, B., Nusbaum, C., Zody, M. C., Baldwin, J., Devon, K., Dewar, K., Doyle, M., FitzHugh, W., Funke, R., Gage, D., Harris, K., Heaford, A., Howland, J., Kann, L., Lehoczky, J., LeVine, R., McEwan, P., McKernan, K., et al., *Nature* 2001, *409*, 860–921.

[2] Venter, J. C., Adams, M. D., Myers, E. W., Li, P. W., Mural, R. J., Sutton, G. G., Smith, H. O., Yandell, M., Evans, C. A., Holt, R. A., Gocayne, J. D., Amanatides, P., Ballew, R. M., Huson, D. H., Wortman, J. R., Zhang, Q., Kodira, C. D., Zheng, X. Q. H., Chen, L., Skupski, M., et al., *Science* 2001, *291*, 1304–1354.

[3] Jacobson, S. C., Hergenroder, R., Koutny, L. B., Ramsey, J. M., *Anal. Chem.* 1994, *66*, 1114–1118.

[4] Paegel, B. M., Yeung, S. H. I., Mathies, R. A., *Anal. Chem.* 2002, *74*, 5092–5098.

[5] Pal, R., Yang, M., Lin, R., Johnson, B. N., Srivastava, N., Razzacki, S. Z., Chomistek, K. J., Heldsinger, D. C., Haque, R. M., Ugaz, V. M., Thwar, P. K., Chen, Z., Alfano, K., Yim, M. B., Krishnan, M., Fuller, A. O., Larson, R. G., Burke, D. T., Burns, M. A., *Lab on a Chip* 2005, *5*, 1024–1032.

[6] Blazej, R. G., Kumaresan, P., Mathies, R. A., *Proc. Natl. Acad. Sci. USA* 2006, *103*, 7240–7245.

[7] Easley, C. J., Karlinsey, J. M., Bienvenue, J. M., Legendre, L. A., Roper, M. G., Feldman, S. H., Hughes, M. A., Hewlett, E. L., Merkel, T. J., Ferrance, J. P., Landers, J. P., *Proc. Natl. Acad. Sci. USA* 2006, *103*, 19272–19277.

[8] Liu, P., Mathies, R. A., *Trends Biotechnol.* 2009, *27*, 572–581.

[9] Hopwood, A. J., Hurth, C., Yang, J. N., Cai, Z., Moran, N., Lee-Edghill, J. G., Nordquist, A., Lenigk, R., Estes, M. D., Haley, J. P., McAlister, C. R., Chen, X., Brooks, C., Smith, S., Elliott, K., Koumi, P., Zenhausern, F., Tully, G., *Anal. Chem.* 2010, *82*, 6991–6999.

[10] Liu, P., Li, X., Greenspoon, S. A., Scherer, J. R., Mathies, R. A., *Lab on a Chip* 2011, *11*, 1041–1048.

[11] Fredlake, C. P., Hert, D. G., Root, B. E., Barron, A. E., *Electrophoresis* 2008, *29*, 4652–4662.

[12] Ogston, A. G., *Trans. Faraday Soc.* 1958, *54*, 1754–1757.

[13] Lunney, J., Chrambach A, Rodbard, D., *Anal. Biochem.* 1971, *40*, 158–173.

[14] Rodbard, D., Chrambach A, *Anal. Biochem.* 1971, *40*, 95–134.

[15] Lumpkin, O. J., Dejardin, P., Zimm, B. H., *Biopolymers* 1985, *24*, 1573–1593.

[16] Slater, G. W., Noolandi, J., *Biopolymers* 1986, *25*, 431–454.

[17] Duke, T., Viovy, J. L., Semenov, A. N., *Biopolymers* 1994, *34*, 239–247.

[18] Luckey, J. A., Norris, T. B., Smith, L. M., *J. Phys. Chem.* 1993, *97*, 3067–3075.

[19] Heller, C., *Electrophoresis* 2000, *21*, 593–602.

[20] Slater, G. W., Kenward, M., McCormick, L. C., Gauthier, M. G., *Curr. Opin. Biotechnol.* 2003, *14*, 58–64.

[21] Slater, G. W., *Electrophoresis* 1993, *14*, 1–7.

[22] Tinland, B., *Electrophoresis* 1996, *17*, 1519–1523.

[23] Pluen, A., Tinland, B., Sturm, J., Weill, G., *Electrophoresis* 1998, *19*, 1548–1559.

[24] Tinland, B., Pernodet, N., Pluen, A., *Biopolymers* 1998, *46*, 201–214.

[25] Pernodet, N., Tinland, B., Sturm, J., Weill, G., *Biopolymers* 1999, *50*, 45–59.

[26] Nkodo, A. E., Tinland, B., *Electrophoresis* 2002, *23*, 2755–2765.

[27] Grossman, P. D., Menchen, S., Hershey, D., *Genet. Anal.-Biomol. Eng.* 1992, *9*, 9–16.

[28] Yarmola, E., Sokoloff, H., Chrambach, A., *Electrophoresis* 1996, *17*, 1416–1419.

[29] Brahmasandra, S. N., Burke, D. T., Mastrangelo, C. H., Burns, M. A., *Electrophoresis* 2001, *22*, 1046–1062.

[30] Djouadi, Z., Bottani, S., Duval, M. A., Siebert, R., Tricoire, H., Valentin, L., *Electrophoresis* 2001, *22*, 3527–3532.

[31] Ugaz, V. M., Burke, D. T., Burns, M. A., *Electrophoresis* 2002, *23*, 2777–2787.

[32] Lo, R. C., Ugaz, V. M., *Electrophoresis* 2006, *27*, 373–386.

[33] Luckey, J. A., Smith, L. M., *Anal. Chem.* 1993, *65*, 2841–2850.

[34] Kamahori, M., Kambara, H., *Electrophoresis* 1996, *17*, 1476–1484.

[35] Karger, A. E., *Electrophoresis* 1996, *17*, 144–151.

[36] Heller, C., *Electrophoresis* 1999, *20*, 1978–1986.

[37] Fredlake, C. P., Hert, D. G., Kan, C. W., Chiesl, T. N., Root, B. E., Forster, R. E., Barron, A. E., *Proc. Natl. Acad. Sci. USA* 2008, *105*, 476–481.

[38] Buchholz, B. A., Barron, A. E., *Electrophoresis* 2001, *22*, 4118–4128.

[39] Chiesl, T. N., Shi, W., Barron, A. E., *Anal. Chem.* 2005, *77*, 772–779.

[40] Mercier, J. F., Slater, G. W., *Electrophoresis* 2006, *27*, 1453–1461.

[41] Menchen, S., Johnson, B., Winnik, M. A., Xu, B., *Electrophoresis* 1996, *17*, 1451–1459.

[42] Yarmola, E., Calabrese, P. P., Chrambach, A., Weiss, G. H., *J. Phys. Chem. B* 1997, *101*, 2381–2387.

[43] Deutsch, J. M., *Science* 1988, *240*, 922–924.

[44] Deutsch, J. M., Madden, T. L., *J. Chem. Phys.* 1989, *90*, 2476–2485.

[45] Schwartz, D. C., Koval, M., *Nature* 1989, *338*, 520–522.

[46] Chiesl, T. N., Putz, K. W., Babu, M., Mathias, P., Shaikh, K. A., Goluch, E. D., Liu, C., Barron, A. E., *Anal. Chem.* 2006, *78*, 4409–4415.

[47] Randall, G. C., Doyle, P. S., *Phys. Rev. Lett.* 2004, *93*, 058102.

[48] Popelka, S., Kabatek, Z., Viovy, J. L., Gas, B., *J. Chromat. A* 1999, *838*, 45–53.

[49] Li, A. R., Chen, X. J., Ugaz, V. M., *Anal. Chem.* 2010, *82*, 1831–1837.

[50] Viovy, J. L., *Rev. Mod. Phys.* 2000, *72*, 813–872.

[51] Tinland, B., Pluen, A., Sturm, J., Weill, G., *Macromolecules* 1997, *30*, 5763–5765.

[52] Barron, A. E., Soane, D. S., Blanch, H. W., *J. Chromat. A* 1993, *652*, 3–16.

[53] Barron, A. E., Blanch, H. W., Soane, D. S., *Electrophoresis* 1994, *15*, 597–615.

[54] Slater, G. W., Mayer, P., Grossman, P. D., *Electrophoresis* 1995, *16*, 75–83.

[55] Zhou, H. H., Miller, A. W., Sosic, Z., Buchholz, B., Barron, A. E., Kotler, L., Karger, B. L., *Anal. Chem.* 2000, *72*, 1045–1052.

[56] Koutny, L., Schmalzing, D., Salas-Solano, O., El-Difrawy, S., Adourian, A., Buonocore, S., Abbey, K., McEwan, P., Matsudaira, P., Ehrlich, D., *Anal. Chem.* 2000, 72, 3388–3391.

